Chalcogenide Letters Vol. 18, No. 11, November 2021, p. 701 - 715

Studies on copper indium selenide/Zinc sulphide semiconductor quantum dots for solar cell applications

P. J. S. Babu[a,*], T. S. Padmanabhan[a], M. I. Ahamed[b], A. Sivaranjani[c]
[a]*Department of Electrical and Electronics Engineering, E.G.S. Pillay Engineering College, Nagapattinam – 611002, Tamilnadu, India*
[b]*Department of Electronics and Communication Engineering, E.G.S. Pillay Engineering College, Nagapattinam – 611002, Tamilnadu, India*
[c]*Department of Micro-Nano Mechanical Science & Engineering, Graduate School of Engineering, Nagoya University, Nagoya 464-8603, Japan*

Despite dedicated efforts to develop efficient quantum dot sensitized (QDS) photovoltaic cells, the efficiency of these cells still lags behind their theoretical value. In order to increase photo conversion efficiency, the extant methods are predominantly focus on modifying the band gaps of quantum dots and optimizing the interfaces of cell components to increase light utilization capacity. In this study, we have designed and investigated QDS solar cells using Copper Indium Selenide ($CuInSe_2$ or simply CIS) as a quantum dot absorber. In order to achieve tunable bandgap, increased photoluminescence, reduced density of surface defect state and higher light-harvesting efficiency, the $CuInSe_2$ is alloying with Zinc sulfide (ZnS) to design Copper Indium Selenide-Zinc sulfide (CISZS) quantum dots. The resulting CISZS sensitizer exhibits improved photoelectric characteristics and greater chemical stability. The performance of the CIS and CISZS solar cells is evaluated individually through Silvaco-Atlas simulation software in terms of measures such as power conversion efficiency, open-circuit voltage (Voc), the density of short-circuit current (Jsc) and fill-factor (FF). The CISZS-based solar cells show an average conversion efficiency of 23.5% (i.e., 4.94% higher than the efficiency of CIS solar cell) with Voc = 0.596V, Jsc = 23.61mA/cm^2 and FF = 0.84 under AM 1.5G with a power density of 100mW/cm^2. The achieved power conversion efficiency indicates the greatest performances of the QDS solar cells. These non-toxic photovoltaic devices reveal better optical and electrical properties than toxic lead and cadmium chalcogenide quantum dots absorbers.

(Received September 9, 2021; Accepted November 16, 2021)

Keywords: CIS quantum dots, CISZS quantum dots, Conversion efficiency, Photoelectric properties, Solar cells

1. Introduction

The global electrical energy demand is estimated around 23,398 TWh in 2018, where 18,718 TWh (i.e., 80%) of this energy is generated by fossil fuels [1]. It is projected that by 2050 our global electricity consumption will be doubled due to the industrial revolution and the exponential growth in the world population [2]. The increasing energy crisis, and extreme shortage of natural energy resources, environmental pollution and climate change requires assiduous efforts from researchers to find effective and lucrative renewable energy alternatives to meet future energy needs. Energy generation from renewable energy sources like solar, wind, geothermal and biogas act an imperative role in electrical grids for facilitating sustainable power supply [3]. Nowadays, there is a growing interest in photovoltaic (PV) system and inverter [4, 5] since it provides the most important and efficient solution to surge in electricity demand and serious ecological impacts. Our planet is unceasingly receiving 3 million exajoules solar energy per year, whereas 0.01% of this energy is enough to meet the global electricity demand. Although solar energy generation has become a world trend, still there are significant challenges and issues related

* Corresponding author: sureshbabu@egspec.org

to handling the energy crisis with the maximum realizable performance and the ever-increasing urge for renewable energy solutions.

In the recent years nanomaterials-based solar cells are the most reliable and inexpensive devices with high theoretical photo conversion efficiency (PCE). To improve the realizable efficiency of PV systems used for commercial applications, innumerable approaches have been studied mainly from material perspectives. Hence, research on the application of PV technologies based on nanomaterials is of strategic and realistic significance. At present, quantum dot (QD) is a topic of intense research activity aiming at a wide variety of commercial applications [6]. Adaptable near-infra-red optical absorption [7], higher absorption constant [8], hot electron injection [9], multiple exciton generation [10], lower cost, and rationally higher PCE [11] are some of the attractive characteristics of the quantum dot materials. However, the process of material selection and their process are crucial to realize the improved photo conversion efficiency. Unfortunately, most of the best-realized cell enactments are all based on QDs comprising heavy toxic components such as lead [12, 13] or cadmium [14, 15] chalcogenides. These toxic metals considerably limit their potential applications in commercial developments owing to environmental and health hazards. Besides, the photo conversion performance of existing QDS cells is poor, and it remains to be enhanced for a potential application.

Therefore, identifying effective and toxic-free sensitizers for practical solar cells is still an urgent task. In this respect, recently, few near-infra-red Copper-based quantum dots have been studied because of their excellent photoelectric and eco-friendly properties. There are unremitting efforts towards constructing an efficient QDS cell since 1990 when the photovoltaic effect was observed during the measurement of specific conductance of an organic layer [16]. In 1994, for the first time, Vogel et al. fabricated a solar cell using a sensitized mesoporous TiO_2 as photo anode and cadmium sulfide as a QDs absorber [17]. The efficiency of this photovoltaic device is measured through a three-electrode formation and around 6% of efficiency was reported in this work. The non-stoichiometric proportions of copper and indium materials to form CIS cell is optimized by Wang et al. to achieve PCE of 8.54%, which is the best performance for the Cu-based photovoltaic cells [18]. Yang et al. proposed a double TiO_2 electrode configuration and a mesh-structured semi-transparent Cu_2S as CE [19]. The proposed cell exhibits around a 12% rise in conversion efficiency. Conversely, the light-harvesting response of the device is deprived. Du et al. proposed an alloyed Zn-Cu-In-Se sensitizer. The authors deposited Zn-Cu-In-Se and CdSe on mesoporous TiO_2. This cell realized conversion efficiency up to 11.6% [20]. But, the meager loading of quantum dot absorbers affects the electronic coupling between TiO_2 and absorber and thus affects the efficiency of the cell.

Zhang et al. proposed a QDS cell with Zn–Cu–In–Sn as an absorber. This cell introduced a new level of conversion efficiency (14.02%) [21]. Continuously reducing the bandgap of QDs absorber to improve light utilization efficiency leads to a considerable loss in open-circuit voltage and consequently reduces the cell efficiency. Wang et al. tested the electrolytic reduction at the electrolyte/photoanode contact by illuminating the CE (i.e., CuS). This enables a 15% of conversion efficiency, which is attributed to plasmonic resonance absorption and photo-thermal effect [22]. Sobayela et al. simulated a copper indium gallium selenide (CIGS) photovoltaic device with a window layer using WS_2 to realize PCE of 26.4% [23]. The empirical results prove that the projected cell is less temperature-sensitive as related to typical silicon-based photovoltaic cells. Even though the QDS photovoltaic devices are achieving PCE up to 26.4% [23], they are still far behind the traditional heterojunction-based photovoltaics (38.8%) [24]. Immense research is being conducted to enhance cell efficiency. Multifaceted processes such as light absorption, carrier separation, and carrier mobility across multiple junctions are involved in these cells. Hence, optimization of various cell elements such as selection of QDs materials, their quality, and dimension [25, 26], type of electron and hole conducting materials, electrolyte, CE material [27], etc. have become intense research focus. Few other techniques including surface passivation [28], light trapping for higher absorption [29], implementing whispering gallery resonators in the electrodes [30], etc. are being explored for enhancing the cell performance.

Herein, we explored Copper-based QDS cells through a precise numerical simulation study. We selected CIS and CISZS materials as QDs absorbers. The selected CIS shows exclusive characteristics of a high molar extinction constant ($\sim 10^5$ cm^{-1}), a wider Bohr radius (10.6 nm), and

a relatively narrow bandgap (1.84 eV). Furthermore, it can increase the light-absorption range . In order to realize higher photoelectric characteristics and greater chemical stability, the CIS is alloyed with ZnS to form CISZS quantum dots. CISZS exhibits superior photoelectric properties such as bandgap tuning, increased photoluminescence, reduced density of surface defect state, higher light-harvesting capacity, etc. We also selected Titanium dioxide (TiO_2) as an electron transport material, a polysulfide electrolyte as a hole transport material, and Cu_2S as the counter electrode. We used Silvaco-Atlas simulation software to analyze and optimize the electrical parameters of CIS and CISZS solar cells. The performance of CIS and CISZS cells is evaluated through the appropriate performance measures.

2. Structure of Proposed QDs Solar cell

Amongst all photovoltaic devices, QDS cells became well-known for higher PCE in which a large size of porous electron transportation material is employed as the active electrode. The measured performance enhancement was ascribed to the large geometrical dimension of the photoanode, supporting the formation of a monolayer of appropriate QDs material on the surface. A nanostructured semiconductor electrode with a large surface area and wide bandgap is selected as the electron-conducting material. The large geometrical dimension of the EC creates more opportunities to deposit enough amount of QDs material for absorbing incident photons. A polysulfide redox electrolyte is employed as a hole conductor. The sensitizer absorbs incident radiation and generates excitons. This electron is detached at the interface of the EC/QDs absorber and it is transported to EC, whereas the hole is transported to HC from sensitizer, possibly at a later time as given in Figure 1. A QDS solar cell contains many elements, which need to be cautiously chosen and engineered to fabricate solar cells with improved photovoltaic performance.

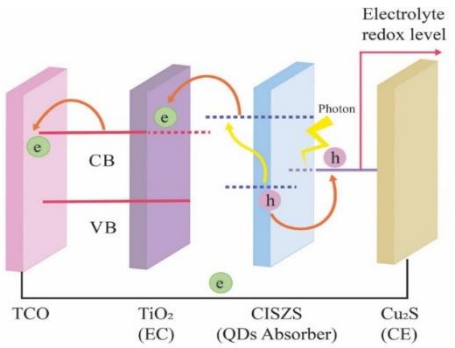

Fig. 1. Structure of CISZS-based QDS photovoltaic cell.

2.1. Quantum dots absorber

The choice of suitable QDs material for fabricating an effective photovoltaic device is vital. Shockley and Queisser measured the maximum detailed balance efficiency of a photovoltaic device [31]. This detailed balance PCE relies intensely on the absorber band gap. Similarly, Klimov measured detailed balance efficiency for QDs sensitizer-based devices [32] as given in Figure 2.

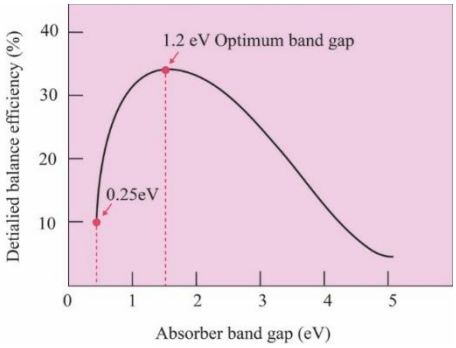

Fig. 2. Absorber bandgap versus detailed balance efficiency.

Figure 2 illustrates that there is a robust relationship between detailed balance efficiency and absorber bandgap. Hence, the bandgap of quantum dots sensitizer is of utmost significance for the construction of proficient PV devices as the photons having energy above band offset of QDs absorber will be converted into electric current, and photons possessing energy lower than band offset will be rejected. Klimov et al also demonstrated that 1.2 eV is the optimal bandgap of the excitonic absorber. In QDS cells, extra restraints are placed over band offset since absorbing materials should be capable of injecting electrons to the EC and holes should be transported to HC [33]. Hence, the bandgap of the QDs absorber ought to be greater than the difference between electrolyte redox potential and conduction level of EC [34]. Furthermore, there is a report demonstrating that 0.25 eV of energy is enough to achieve a better electron injection rate [35].

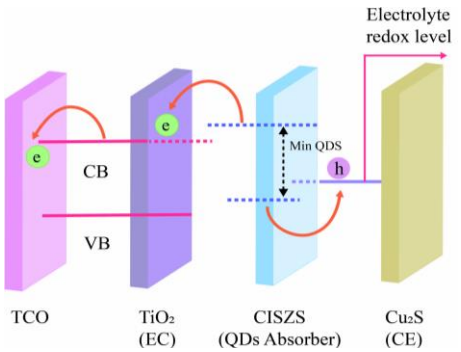

Fig. 3. Minimum bandgap required for QDS material to realize the photovoltaic effect.

The conduction level of absorbing materials should be aligned to 0.25 eV or more than the conduction level of EC material and the valence level of excitonic absorber should be aligned to less than the electrolyte level of HC material. For achieving effective photo-activated electron injection into EC, the conduction level of absorbing materials should be 0.25 eV or more than the conduction level of EC material and the valence level of excitonic absorber should be less than the electrolyte level of HC material. The thermodynamic constraint for electron separation at the interface is that the bandgap should be greater than the binding energy of exciton. In order to realize a better photovoltaic response, the energy level of excitonic absorbing material can be increased through doping, developing core-shell configuration, or alloying various quantum dot absorbers. The doping leads to mid-band states and charge dynamics of excitons generated from doped absorbing materials will be varied from non-doped materials. For instance, enhancement in CIS-based QDS cell with Ga doping is ascribed to the generation of mid-band levels and consequently enables greater carrier lifetime. The generation of mid-gap states of CIS absorber after doping with Gallium is illustrated in Figure 6.

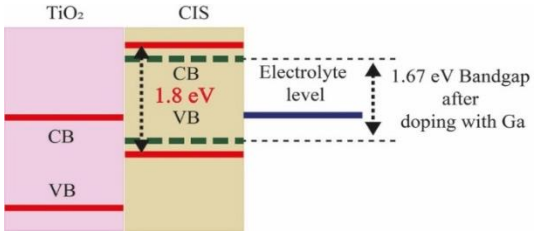

Fig. 4. Formation of mid-gap states in CIS QDs with Ga doping.

The energy level and bandgap of alloyed QDs material strongly hinge on their integral components [36]. For example, the variation in band offset value of CIS material (1.81 eV) after adding with ZnS materials (1.53 eV) is illustrated in Figure 5. Hence, QDS solar cells with alloyed absorbers are widely used to design efficient solar devices with superior photo conversion responses.

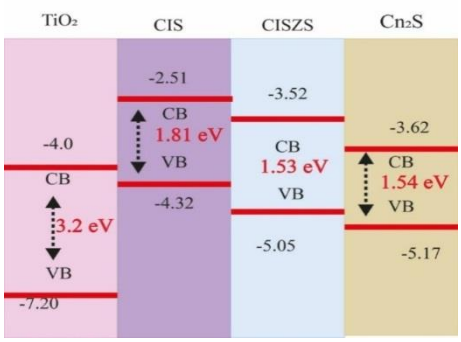

Fig. 5. Illustration of increased energy level by alloying different QDs absorbers.

The practical implementation of quantum dot sensitizers is a difficult endeavor and demands new QD absorbers with appropriate bandgap values, extended carrier lifetimes, and slow carrier dynamics. In this work, we select CIS material as a QDs absorber to fabricate efficient photovoltaic devices due to its increased absorption capacity, superior power conversion efficiency, bandgap grading, low toxicity, and flexibility. In order to achieve bandgap tuning, increased photoluminescence, reduced density of surface defect state, and superior light-harvesting capacity the CIS is alloying with ZnS to design the CISZS quantum dots. The resultant CISZS quantum dots absorber exhibits improved photoelectric characteristics and greater chemical stability. By varying the composition of CIS and ZnS materials, some alloyed $(CIS)_x$-$(ZS)_{1-x}$ quantum dots with adaptable bandgap are obtained and the value x is varied to obtain a Copper/Indium/Selenide composition of 1:1.1:2.1 (approximately equal to the stoichiometric proportion 1:1:2), and CIS-ZS constituent of around 0.6:0.4, 0.7:0.3 and 0.8:0.2 (i.e., $CIS_{0.6}$-$ZS_{0.4}$, $CIS_{0.7}$-$ZS_{0.3}$, and $CIS_{0.8}$-$ZS_{0.2}$). The empirical and simulation results demonstrate that all the CIS and CIS_x-ZS_{1-x} sensitizers show chalcopyrite form of structure and the band offset value of the QDs absorbers are calculated as 1.53 eV (CISZS), 1.41 eV ($CIS_{0.8}$-$ZS_{0.2}$), 1.48 eV ($CIS_{0.7}$-$ZS_{0.3}$), and 1.50 eV ($CIS_{0.6}$-$ZS_{0.4}$).

2.2. Electron conductor

Electron conducting materials play a central role in the working of QDS solar cells. It receives excitons from QDs material and transfers these excitons to TCO contact. For effective receipt of excitons from QDs material, an appropriate bandgap between the QDs absorber and EC is mandatory. Figure 6 illustrates the necessity of an appropriate bandgap at the EC/QDs interface. For effective electron acceptance, the conduction band of EC should be less than that of QDs material. Also, the rate of injection increases up to a bandgap of 1 eV and becomes almost

invariant after that. Interested readers can refer [37] for more information about interfacial charge transfer.

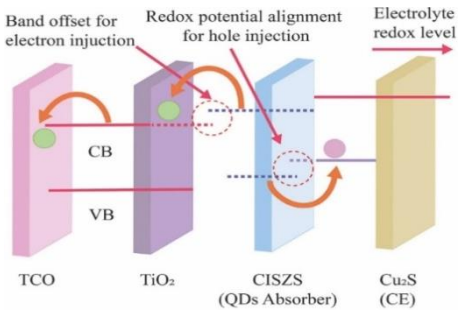

Fig. 6. Bandgap requirement for transferring excitons from QDs material to EC.

Figure 6 displays the required energy bands orientation for EC with sensitizers conduction level for effective electron transportation and the electrolyte level orientation with valence band of sensitizers for effective hole transportation. Moreover, the material used as EC should be photo-stable and have a higher band offset value. The photo-stability property of EC guarantees the effective operation of the cell under radiation and higher bandgap guarantees that a large number of photons in radiations are absorbed by QDs material and not by EC. The absorption of photons at EC is detrimental since it stimulates recombination between redox HC and EC. The electron conduction capacity of EC is an additional critical factor for competent QDS solar cells as the injected photons are gathered at contact through transmission. To realize higher power conversion efficiency, the injected excitons should be gathered at contact before they recombine. Therefore, the reduced conductivity may cause loss of excitons due to recombination and causing the deprived performance. Numerous wide bandgap semiconductors are studied earlier with changing architecture and morphology to fabricate effective QDS cells.

Few well-known EC materials used for QDS cells are Zinc oxide (ZnO), Titanium oxide (TiO_2), Tin oxide (SnO_2), Zinc titanate ($Zn_2Ti_3O_8$), Zinc stannate (Zn_2SnO_4), and Strontium titanate ($SrTiO_3$). Some of the other large bandgap materials such as Ta_2O_5 and Nb_2O_5 are also used as EC in QDS cells but their photovoltaic performance is poor as compared to TiO_2 . In this work, we used TiO_2 as an electron transport material. It is an extensively studied and utilized EC material owing to its promising features including abundance, cheapness, and non-toxicity. TiO_2 is a transition metal oxide with a rich orbital contribution to valence and conduction level. This feature reduces recombination possibilities and increases the carrier lifetimes efficiently. TiO_2 exists in three forms viz. Brookite (with a bandgap of 3.26 eV), rutile (with a bandgap of 3.05 eV), and Anatase (with a bandgap of 3.23 eV). Amongst these phases, rutile is the most stable and widely utilized for a variety of applications. In this study also, we use the rutile form of TiO_2 nanoparticles for the preparation of electron conductor.

2.4. Hole conductor

Hole conductor or hole transport material is another important component of QDS cells. After absorbing solar radiation, quantum dots material generates excitons and injects into EC and therefore, quantum dots material is oxidized. HC is responsible to accept holes from oxidized quantum dots material. If this hole acceptance rate is low or HC material is having the deprived hole movement, then it will upturn the recombination rate and lead to decreased cell performance. To design QDS solar cell, HC materials can be used in the form of liquid, semi-solid, and solid. Generally, liquid HC is used in QDS cells in form of a redox electrolyte. The most important redox electrolytes used in QDS cells including Iodide electrolyte (I^-/I^{3-}), Polysulfide electrolyte (S^{2-}/S_x), Ferrocene electrolyte ($Fe(CN)_6^{3-}/Fe(CN)_6^{4-}$), Cobalt-based electrolyte, etc. Solid HCs are used to alleviate the leakage issues related to liquid hole conducting materials. Selecting suitable HC material in the mesoporous electrode is an important task. Spiro-OMeTAD is one of the widely used solid hole conductors in QDS solar cells [38].

In QDS cells with gel electrolyte, the liquid polysulfide hole conducting material is transformed into semi-solid form. These electrolytes are pigeonholed by a definite temperature wherein quasi-solid electrolyte is transformed into liquid form. This factor is utilized to calculate the intrinsic stability and gelation strength of the semi-solid electrolyte. A report proved that the utilization of quasi-solid hole conductors in QDS cells is achieved through gelating agents like konjac glucomannan, poly (polypropylene glycol), dextran, 12-hydroxy steric acid, and poly acrylamide-bis-acrylamide [39]. The solid and semi-solid hole conductors increase the stability of solar cells, but with slightly lower efficiency related to polysulfide liquid electrolytes [40]. Hence, this study uses polysulfide electrolyte (S^{2-}/S_x) as a hole conducting material.

2.5. Counter electrode

CE provides catalytic action for the effective reduction of hole conducting material. The electrolyte reduction takes place on the surface of the counter electrode. Therefore, the CE must have more electrochemical catalytic action with a low resistance to decrease the redox potential of the hole conductor. If CE is not sufficiently catalytic, it will reduce electron transport efficiency and increase the impedance at CE/electrolyte interface. This impedance leads to reduced fill factor and consequently poor performance [41]. In earlier studies, Pt was employed as a CE owing to its compatibility with the I^{3-}/I^{-} electrolyte. Conversely, the interface resistance is comparatively high, which hampers the cell performance considerably. Recently, it is witnessed that Pt was not exhibiting effective catalytic properties for S^{2-}/S_x electrolyte and higher impedance is observed at CE/redox interface, resulting in poor cell performance [41]. Several materials such as NiS, Au, and Cu_2S are used as CE to realize improved photovoltaic performances. Among them, NiS and Au are appropriate for the S^{2-}/S_x but introduce large resistance at the interface, therefore controlling the carrier mobility from CE to hole conductor and decrease the performance of QDS cells. NiS electrolyte has been explored for enhanced outcomes, but they contaminate the CE and hole conducting material, which hampers the long-term working of the cell. Cu_xS and its composites have greater absorption capacity and electrochemical stability, which cause performance improvement, so they have been extensively employed as CE material in several QDS photovoltaic devices [42]. Herein, we select Cu_2S as a counter electrode for polysulfide electrolytes to achieve the optimal photovoltaic performance.

3. Theoretical modelling and synthesis of QDs

In this section, we have described the modelling and fabrication details of QDS solar cells with CIS and CISZS quantum dot-sensitized TiO_2 photoanodes. In this study, we have designed and simulate four QDS solar cells using CIS and $(CIS)_x$-$(ZS)_{1-x}$. These cells consist of wide bandgap QDs materials, which are coated on a TCO, polysulfide electrolyte, and CE materials. First, we have simulated QDS solar cells using Sivalco-Atlas software. We have illuminated the cell using AM 1.5G radiation with a power density of $100mW/cm^2$ to measure the photovoltaic response of the cell. Then, we have fabricated the QDS solar cell to measure the photoelectrical response of the cell in terms of designated performance measures.

3.1. Solar cell modelling

As quantum dots photovoltaic devices are made of thin layers, a one-dimensional modelling approach is enough to calculate the efficiency of these cells. The electrical properties of solid-state devices are defined by Poisson's equation as given below:

$$\nabla^2\psi_{(x,y,z)} = -\frac{\rho}{\epsilon_0} \rightarrow \frac{\partial^2\psi_x}{\partial x^2} = \frac{q}{\epsilon}\left[e_{(x)} - \hbar_{(x)}\right] \tag{1}$$

where ψ represents scalar electrical potential, q represents unit charge, ϵ is the dielectric constant of the material, and $\hbar$ and e are the density of hole and electron, correspondingly. Also, the continuity equations for holes and electrons are defined as follow:

$$\frac{\partial \hbar}{\partial t} = R_{gen} - R_{recom} - \frac{1}{q} \times \frac{\partial J_{\hbar}(x)}{\partial x} \tag{2}$$

$$\frac{\partial e}{\partial t} = R_{gen} - R_{recom} + \frac{1}{q} \times \frac{\partial J_{e}(x)}{\partial x} \tag{3}$$

where R_{gen}, R_{recom}, $J_{\hbar}$, and J_e are generation rate, recombination rate, hole current density, and electron current density, correspondingly. A strong electric potential is created across the semiconductor material due to the dissimilarity between the high work function of two electrodes; hence, the charge carriers get drift velocity. It is impossible to solve these differential equations analytically due to the robust relationship that exists between the charge density and the electric field. Hence, we exploited the Silvaco-Atlas simulator to resolve those equations [43]. This software calculates the electrical properties of photovoltaic devices by simulating the movement of carriers across a 2D grid where one particular dimension is invariant for all layers. To simulate the intended photovoltaic devices, we need to define the parameters of each layer in the device individually.

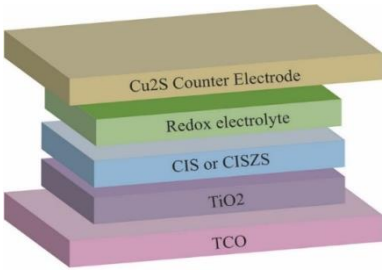

Fig. 7. Layered configuration of the proposed QDS solar device.

To model the proposed QDS cell, we selected fluorine-doped tin oxide (FTO) layer as a TCO substrate with a 5µm thickness and 3×10^{20}cm^{-3} n-type doping concentration. We selected TiO_2 as electron transport material, polysulfide electrolyte (S^{2-}/S_x) solution as a HC material, and Cu_2S as CE. The layered architecture of the proposed QDS cell is given in Figure 7. We obtained the simulation parameters of TiO_2 from [44]. To simulate selected QDs absorbers and CE materials, we utilized the SOPRA database incorporated in the Silvaco software. The standard parameters selected for modelling of the proposed cell are given in Table 1.

Table 1. Standard parameters utilized to model solar cell.

Parameter	**TiO_2**	**CIS**	**CISZS**	**Cu_2S**
Thickness (µm)	10.0	5.0	5.0	4.0
Bandgap energy, Eg (eV) at 300 K	3.2	2.39	1.02	3.60
Electron affinity (eV)	4.20	4.30	4.2	4.13
Dielectric ratio	10	15.2	13.5	8.28
Acceptor/donor doping Na/Nd (cm^{-3})	1×10^{17}	1×10^{18}	1×10^{18}	5×10^{16}
Valence band effective density of states N_v(cm^{-3})	6×10^{17}	7×10^{18}	1.5×10^{19}	2.4×10^{19}
Conduction band effective density of states N_c(cm^{-3})	2×10^{17}	4.7×10^{17}	6.6×10^{17}	1.7×10^{18}
Lifetime (el) (s)	1×10^{-9}	1×10^{-9}	4.4×10^{-9}	2×10^{-8}
Lifetime (ho) (s)	2×10^{-8}	2×10^{-8}	4.4×10^{-9}	6×10^{-8}

The proposed cell is illuminated by a source of AM1.5G with 100mW/cm^2 power density as given in Figure 8. Silvaco resolves Poisson's equation as well as electron and hole continuity equations. In order to simulate the motilities of charge carriers, we used the low-field concentration-dependent mobility approach and the Shockley-read-hall recombination method. Auger model is selected to represent bulk and interface recombination velocities.

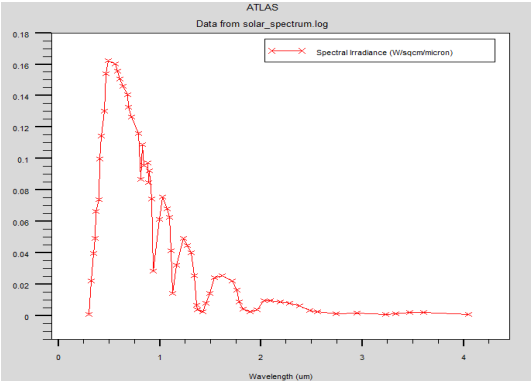

Fig. 8. AM1.5G solar spectrum.

3.1.1. Performance metrics

We assessed the effectiveness of the developed photovoltaic device in terms of performance measures such as the open-circuit voltage, density of short-circuit current, fill factor, incident photon conversion efficiency, and absorbed photon conversion efficiency. The highest obtainable voltage from a solar device is defined as open-circuit voltage. It is defined in Equation (4).

$$V_{oc} = \left(\frac{nkT}{q}\right) \times \ln\left(\frac{I_L}{I_o}\right) + 1 \tag{4}$$

where $\frac{kT}{q}$ is the thermal voltage, n represents ideality factor, I_L denotes light generated current, and I_o is dark saturation current. The short-circuit current is defined as the maximum current supplied by a photovoltaic device and befalls at zero voltage. It is generated by photo-excited carriers and can be defined in Equation (5).

$$J_{SC} = I_o \left[\exp\left(\frac{qV}{nkT}\right) - 1\right] - I_L \tag{5}$$

The fill factor is a quality metric of photovoltaic performance. It is defined as the ratio between the maximum obtainable power and the product of short-circuit current and open-circuit voltage. The expression for the FF can be defined as in Equation (6).

$$FF = V_{oc} - \ln\left(\frac{V_{oc} + 0.72}{V_{oc} + 1}\right) \tag{6}$$

The measure IPCE is used to analyze the light-harvesting and the electron emission capacity of the sensitizer. It can be calculated as the following Equation (7).

$$IPCE = \eta_{LH} \times \eta_{EI} \times \eta_{CC} \tag{7}$$

where η_{LH} represents light-harvesting efficiency, η_{EI} denotes electron-injection efficiency and η_{CC} is carrier collection efficiency. IPCE can be calculated by Equation (8).

$$\eta_{LH}(\lambda) = 1 - 10^{-Abs(\lambda)} \tag{8}$$

The performance measure APCE is employed to analyze the conversion of the absorbed photon to electric energy. It can be calculated using the following Equation (9).

$$APCE = \frac{IPCE}{\eta_{LH}} \tag{9}$$

3.2. QDs Solar cell synthesis

To synthesis the proposed QDS solar cell, Copper (I) iodide (19mg, 0.1mmol) and Indium (III) acetate (29.2mg, 0.1mmol) are dissolved into Oleylamine (4ml) in a flask. This blend is degassed at 180°C using Argon flow. Now, Se stock solutions (2mmol of Se dissolved in 1ml of diphenylphosphine (DPP)) are added into the blend and remained at this temperature for 10 minutes. Then, the mixture is cooled at room temperature and dispersed in Toluene. Additional decontamination is performed by centrifugation and precipitation process using acetone. The graded $CIS_{0.8}$-$ZS_{0.2}$ QDs absorber is prepared in the same way by adding Copper (I) iodide, Indium (III) acetate, and Zinc (II) acetate (11mg, 0.05mmol) in consort with Oleylamine, subsequently injecting Se stock solutions into the flask at 180℃. $CIS_{0.7}$-$ZS_{0.3}$ and $CIS_{0.6}$-$ZS_{0.4}$ are obtained by adding more amount of Zinc (II) acetate and sulfur powder. The final composition is verified through inductively coupled plasma mass spectrometry (ICP) testing.

TiO_2 photoanode is fabricated with 5±0.5µm light scattering layer and 10±0.5µm transparent layer. Using bifunctional molecules of mercaptopropionic acid (MPA), the original Oleylamine-capped oil-soluble QDs material is converted into water-soluble in order to enable ligand exchange. A thin layer of MPA-covered water-soluble absorbing material (5µm thickness) is connected to the photoanode layer by pipetting the quantum dot aqueous solution over the photoanode layer and remaining stationary for 2 hours. A thin film of ZnS is coated on the surface of EC electrode by dipping it into 0.1 M Na_2S aqueous solutions and 0.1 M Zinc (II) acetate alternately for 4 cycles. To end, the photovoltaic devices are assembled by arranging the TiO_2 electrode and Cu_2S using a binder fastener and parted by a 60-µm Scotch spacer. Then the solar cell is filled with polysulfide electrolyte with a composition of 0.5 M S powder, 2.0 M Na_2S, and 0.2 M KCl).

4. Results and discussion

The major objective of this work is to design and simulate solar cells using QDs materials including CIS and CISZS. Besides, we analyzed the electrical and optical properties of the QDs materials by varying the composition of CIS and ZnS. We formed three different alloyed $(CIS)_x$-$(ZS)_{1-x}$ quantum dots with adaptable bandgap are obtained and the x value is varied to obtain a Copper/Indium/Selenide composition of 1:1.1:2.1 (approximately equal to the stoichiometric proportion 1:1:2), and CIS-ZS constituent of around 0.6:0.4, 0.7:0.3 and 0.8:0.2 (i.e., $CIS_{0.6}$-$ZS_{0.4}$, $CIS_{0.7}$-$ZS_{0.3}$, and $CIS_{0.8}$-$ZS_{0.2}$). The simulation results demonstrate that all the CIS and CIS_x-ZS_{1-x} sensitizers show chalcopyrite form of structure and the band offset value of the QDs absorbers are calculated as 1.53 eV (CISZS), 1.41 eV ($CIS_{0.8}$-$ZS_{0.2}$), 1.48 eV ($CIS_{0.7}$-$ZS_{0.3}$), and 1.50 eV ($CIS_{0.6}$-$ZS_{0.4}$).

4.1. Optical Properties of CIS and CISZS QDs

We fabricate the solar cells using CIS and $(CIS)_x$-$(ZS)_{1-x}$ films with varied compositions such as $CIS_{0.6}$-$ZS_{0.}$4, $CIS0_{.7}$-$ZS_{0.3}$ and $CIS_{0.8}$-$ZS_{0.2}$ to observe different optical characteristics. The absorption spectra of the QDs materials CIS, $CIS_{0.6}$-$ZS_{0.}$4, $CIS0_{.7}$-$ZS_{0.3}$, and $CIS_{0.8}$-$ZS_{0.2}$ are shown in Figure 9. Interesting consequences of the absorption statistics are achieved, as given in the absorption spectra, with the absorption onset extending to 900 nm, signifying the greater light-utilization ability for application in solar cells. The greater intensity of the absorption spectra for the QDs material comprising CIS related to CISZS is ascribed to a rise in the QDs absorber concentration. Related to the absorption spectra of CIS, the absorption spectra of CISZS reveal a slight change in the direction of higher wavelengths.

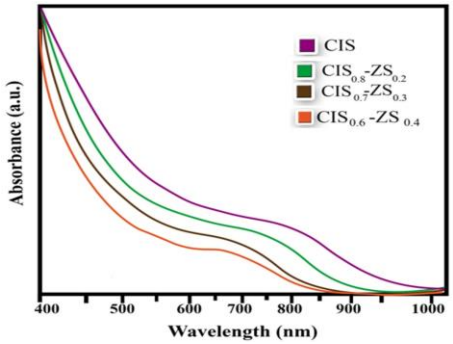

Fig. 9. Normalized absorption spectra of CIS, $CIS_{0.7}$-$ZS_{0.3}$, and $CIS_{0.8}$-$ZS_{0.2}$ QDs absorber

From the optical spectra, it can be inferred that by alloying ZnS with the basic CIS sensitizer, the absorption as well as photoluminescence (PL) emission spectra of the $(CIS)_x$-$(ZS)_{1-x}$ sensitizers exhibit a blue-shift. From these results, we can infer that the $(CIS)_x$-$(ZS)_{1-x}$ materials provide homogeneity or a gradient configuration with ZnS material. Besides, as we combined ZnS with the basic CIS sensitizers, the intensity of PL emission of the $(CIS)_x$-$(ZS)_{1-x}$ materials are amplified progressively, which can be observed from Figure 10. This indicates that the degree of surface defect is less in alloyed $(CIS)_x$-$(ZS)_{1-x}$ sensitizers. Besides, we found that the $(CIS)_x$-$(ZS)_{1-x}$ material could be warehoused for almost 60 days without any photoluminescence intensity quenching, whereas the photoluminescence intensity of CIS is reduced to half of its original value in one week. It is also evidence of the ZnS structure performing as a chemical barrier.

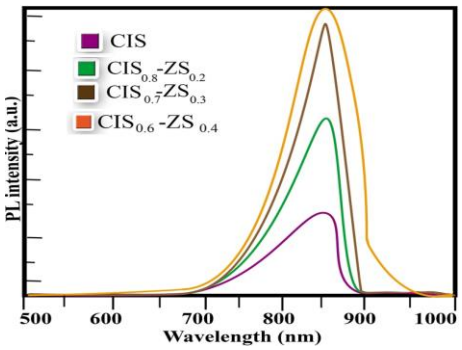

Fig. 10. Photoluminescence emission spectra of QD dispersions at the same concentration

The morphology and size of the nanoparticles in CISZS are analyzed by scanning electron microscopy (SEM) and displayed in Figure 11 (a). The material is primarily made of a huge quantity of nanoparticles with average size of around 8.5nm, and these asymmetrical CISZS nanoparticles are easily combined together. The dimension and microstructure of the quantum dots are further analyzed using transmission electron microscopy (TEM) and high-resolution TEM, correspondingly. In TEM image shown in Figure 11(b), it is observed that the CISZS nanoparticles still accumulated to an extent, though 20 minutes of sonication is used so as to dissolve it before the sample was deposited on the carbon coated copper grid for the TEM analysis. The size is approximately 8–9nm, nearly in line with the measured value from SEM results.

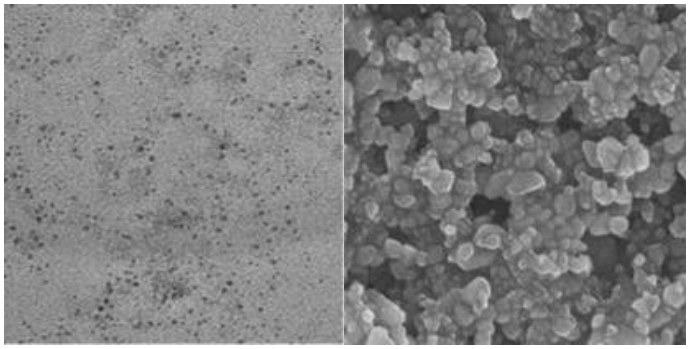

Fig. 11. (a) SEM images of CISZS quantum material; (b) TEM images of CISZS quantum material.

4.2. Photovoltaic performance of CIS and CISZS

To evaluate the photo conversion characteristics of the established devices, the current density-voltage (J-V) measurements, IPCE, and APCE are carried out. The empirical and simulation results are given in Table 2. When relating measured data with simulation results, it is observed that they are very close to each other as shown in Figure 12

Table 2. Photovoltaic performance of proposed cell.

QDS cell	Voc (v)		Jsc (A/cm^2)		FF		PCE (%)	
	Simulation	Experiment	Simulation	Experiment	Simulation	Experiment	Simulation	Experiment
CIS	0.561	0.559	21.46	20.43	0.823	0.817	18.56	17.87
CISZS	0.596	0.586	23.61	22.15	0.839	0.824	23.50	22.14

The photovoltaic performance of TiO_2/CIS/ Polysulfide electrolyte (S^{2-}/S_x)/Cu_2S quantum dots sensitized cell shows increased open circuit voltage (0.561V), short circuit current (21.46A), and fill factor (82.3%). The increased value of Voc and FF increase the PCE of the cell to 21.46%. The CISZS solar cell shows average conversion efficiency of 23.61% with Voc = 0.596V, Jsc = 23.61mA/cm^2, FF = 83.9% under AM 1.5G radiation.

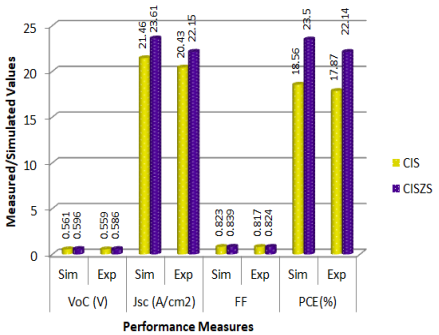

Fig. 12. Comparison of Measured and simulated performance measures of solar cells.

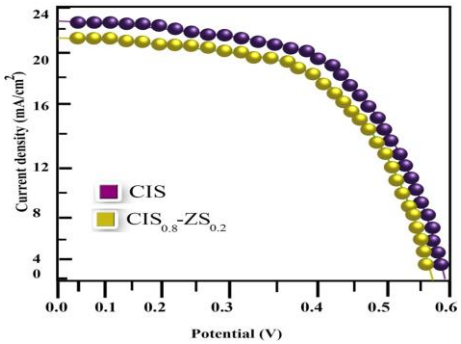

Fig. 13. J−V curves of CIS and CISZS cells.

Figure 13 illustrates density of short circuit current-voltage characteristic curves of the proposed QDS cells. To evaluate the solar spectrum absorption and the electron generation properties, IPCE is investigated and illustrated in Figure 15. The measured value of this external quantum efficiency reveals a robust photovoltaic response with a value of 82% within in the visible region between 400 and 600 nm. The greater IPCE value usually represents the superior absorption characteristic of quantum dots material in the spectral region. From the result, it can be observed that a wider response wavelength range of both CIS and CISZS with increased incident photon conversion efficiency is obtained with remarkably great absorption onset (i.e., beyond 1000nm) and in line with the fluctuating nature of Jsc as perceived in J-V measurement displayed in Figure 14. The maximum IPCE value of the CISZS cell is ~83%. It is slightly more than that of the CIS cell. It can be inferred that the variations in the IPCE value is owing to the higher charge collection efficiency or electron injection efficiency as their light-harvesting efficiency is almost at the same level as designated by the absorption profile given in Figure 9.

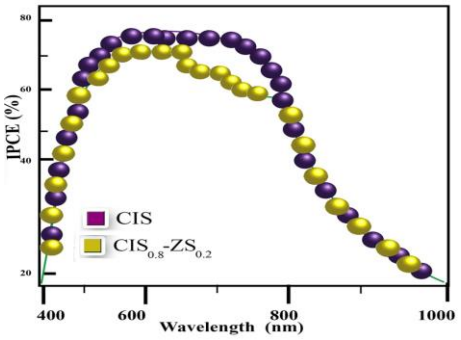

Fig. 14. IPCE curves of CIS and CISZS cells.

APCE is one more vital property of a QDS device. APCE is also utilized to analyze the transformation of the absorbed photon into the current. From Figure 15, we observed that the CISZS cells reveal a higher value of APCE in the range of 400 to 700 nm than that of the CIS solar cell. This discloses that CISZS cells exhibit improved photocurrent conversion performance and alloying ZnS with CIS remarkably increases the enactment of the electron injection and collection.

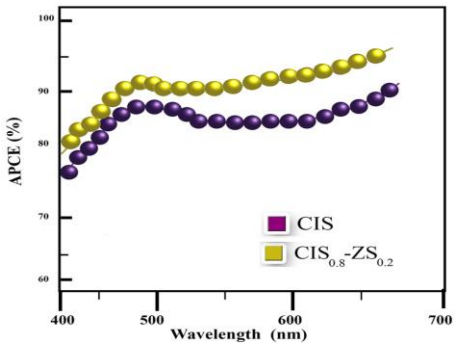

Fig. 15. Absorbed photon-to-electron conversion efficiency (APCE).

5. Conclusion

Copper Indium Selenide-based photovoltaic devices are perceived to be a potential alternative to photovoltaic devices based on cadmium or lead QDs material owing to their low toxicity and superior absorbing capacity. In this work, we synthesis and simulate QDS solar cells using CIS as the quantum dot absorber. In order to achieve bandgap tuning, increased photoluminescence, reduced density of surface defect state, and higher light-harvesting efficiency the CIS is alloying with ZnS to design the CISZS quantum dots. By varying the composition of CIS and ZnS materials, some alloyed $(CIS)_x$-$(ZS)_{1-x}$ quantum dots with adaptable bandgap are obtained. Using the Silvaco-Atlas simulator, we achieve modelling of CIS and CISZS based QDS solar cells under irradiation source of AM1.5G with a power density of 100mW/cm^2. We first simulated CIS and CISZS solar cells individually and then obtain the optical characteristics of each cell for further analysis. To assess the photovoltaic performance of the established cells, the current density-voltage measurements, IPCE, and APCE are calculated.

When relating measured data with simulation results, it is observed that they are very close to each other. Furthermore, the CISZS quantum dots sensitizer exhibits improved photovoltaic characteristics and greater chemical stability. CISZS-based solar cells show average conversion efficiency of 23.5% (i.e., 4.94% higher than the efficiency of CIS solar cell) with the open circuit voltage is 0.596V, the density of short-circuit current is 23.61mA/cm^2, and fill factor is 0.84 under AM 1.5G radiation with a power density of 100mW/cm^2. The achieved power PCE is among the best ones for QDS solar cells and also reveals better optical and electrical properties than that of the toxic lead and cadmium chalcogenide-based quantum dots absorber.

References

[1] Satistia, Net consumption of electricity worldwide in select years from 1980 to 2018, Available online: https://www.statista.com/statistics/280704/world-power-consumption/ (accessed on 5 April 2021)
[2] D. Gielen, F. Boshell, D. Saygin, M.D. Bazilian, N. Wagner, R. Gorini, Energy Strategy Rev. **24**(1), 38 (2019)
[3] J. Kumar, C. R. Majid, M. A., Energy, Sustainability and Society **10**(2), 2020.
[4] G. Chitrakala, N. Stalin, V. Mohan, J. Circuits Sys. Comp. **29**(2), 2050019 (2019).
[5] S. Jeevananthan, R. Madhavan, T. Suresh Padmanabhan, P. Dananjayan, IEEE International Conference on Industrial Technology, 1269 (2006).
[6] S. Higashimoto, T. Nakase, S. Mukai, M. Takahashi, J. Coll. Interf. Sci. **176**(1), (2019).
[7] M. I. Ahamed, K. S. Kumar, E. E. Anand, A. Sivaranjani, J. Ovonic. Res. **16**(4), 245 (2020).
[8] M. I. Ahamed, K. S. kumar, Mater. Sci.-Poland. **37**(1), 108 (2019).
[9] M. Alavi, R. Rahimi, Z. Maleki, M. Hosseini-Kharat, ACS omega **5**(19), 11024 (2020).
[10] L. Hu, Q. Zhao, S. Huang, Nat Commun. **12**, 466 (2021).
[11] P. Xu, X. Chang, R. Liu, L. Wang, X. Li, X. Zhang, X. Yang, D. Wang, W. Lü, Nanoscale

Research Letters **15**(1), (2020).
[12] J. Jiao, Z. Zhou, W. Zhou, S. Wu, Appl. Mater. Sci. Semicond Process. **16**(1), 435 (2013).
[13] R. B. Vasiliev, S. G. Dorofeev, D. N. Dirin, D. A. Belov, Mendeleev Commun. **14**(1), 169 004).
[14] T. Archana, K. Vijayakumar, G. Subashini, A. N. Grace, M. Arivanandhan, R. Jayavel, Mater. Res. Express. **7**(1), 015528 (2020).
[15] A. Ganguly, S. S. Nath, Mater. Sci. Eng. B **255**, 114532 (2020).
[16] B. Gregg, M. Fox, A. Bard, J. Phys. Chem. **94**, 1586 (1990).
[17] R. Vogel, P. Hoyer, H. Weller, J. Phys. Chem. **98**(12), 3183 (1994).
[18] G. Wang, H. Wei, J. Shi, Y. Xu, H. Wu, Y. Luo, D. Li, Q. Meng, Nano Energy **35**, 17 (2017).
[19] Y. Y Yang, Q. X. Zhang, T. Z. Wang, L. F. Zhu, X. M. Huang, Electrochim Acta **88**, 44 2013).
[20] J. Du, Z. Du, J. S. Hu, Z. Pan, Q. Shen, J Am Chem Soc. **138**, 4201 (2016).
[21] H. Zhang, X. Ji, N. Liu, Q. Zhao, Electrochim Acta **327**, 134937 (2019).
[22] F. Wang, H. Wang, X. Liu, D. Wu, K. Jiang, Adv Energy Mater. **8**, 1800136 (2018).
[23] K. Sobayel, M. Shahinuzzaman, N. Amin, M. R. Karim, M. A. Dar, R. Gulf, M. A. Alghoul, K. Sopian, A. K. M. Hasan, Md. Akhtaruzzaman, Solar Energy **207**(1), 479 (2020).
[24] P. T. Chiu, D. C. Law, R. L. Woo, S. B. Singer, D. Bhusari, W.D. Hong, A. Zakaria, J. Boisvert, S. Mesropian, R. R. King, N. H. Karam, 2014 IEEE 40th Photovolt. Spec. Conf. PVSC. 11 (2014).
[25] F. Hetsch, X. Xu, H. Wang, S. V. Kershaw, A. L. Rogach, J. Phys. Chem. Lett. **2**, 1879 11).
[26] D. H. Jara, S. J. Yoon, K. G. Stamplecoskie, P. V. Kamat, Chem. Mater. **26**, 7221 (2014).
[27] H. K. Jun, M. A. Careem, A. K. Arof, Renew. Sustain. Energy Rev. **22**, 148 (2013).
[28] F. Zhao, G. Tang, J. Zhang, Y. Lin, Electrochim. Acta **62**, 396 (2012).
[29] H. Kim, K. Yong, Phys. Chem. Chem. Phys. **15**, 2109 (2013).
[30] T. K. Das, P. Ilaiyaraja, C. Sudakar, ACS Appl. Energy Mater. **1**, 765 (2018a).
[31] W. Shockley, H. J. Queisser, J. Appl. Phys. **32**, 510 (1961).
[32] V. I. Klimov, Appl. Phys. Lett. **89**, 123118 (2006).
[33] G. Yang, Y. Zhu, J. Huang, X. Xu, S. Cui, Z. Lu, Opt. Express. **27**(20), A1338 (2019).
[34] N. T. K. Chung, P.T. Nguyen, H. T. Tung, D. H. Phuc, Molecules **26**, 2638 (2021).
[35] H. Song, Y. Lin, M. Zhou, H. Rao, Z. Pan, X. Zhong **11**, 6202 (2021).
[36] D. K. Smith, J. M. Luther, O. E. Semonin, A. J. Nozik, M. C. Beard, ACS Nano **5**, 183 011).
[37] N. H. Němec, E. Galoppini, H. Imahori, V. Sundstrom, R. J. Groarke, Reference Module in Materials Science and Materials Engineering, (2016).
[38] D. Zhou, T. Zhou, Y. Tian, X. Zhu, Y. Tu, Journal of Nanomaterials, (2018).
[39] Song, Han, Rao, Huashang, Zhong, Xinhua, J. Mater. Chem. A **6**(12), 4895 (2018).
[40] F. Cheng, Y. Ou, G. Liu, L. Zhao, B. Dong, S. Wang, S. Wen, Nanomaterials **9**(5), 783 019).
[41] I. Mora-Seró, S. Giménez, F. Fabregat-Santiago, R. Gómez, Q. Shen, T. Toyoda, J. Bisquert, Acc. Chem. Res. **42**, 1848 (2009).
[42] Y. Zhao, H. Pan, Y. Lou, X. Qiu, J. Zhu, C. Burda, J. Am. Chem. Soc. **131**, 4253 (2009).
[43] ATLAS User's Manual, Device Simulation Software, SILVACO International, Santa Clara, 2012.
[44] Shipra Mital Gupta, Manoj Tripathi, Chin. Sci. Bull. **56**(16), 1639 (2011).